DEUTSCHES ELEKTRONEN-SYNCHROTRON DESY

DESY 90-109
September 1990

Silicon Detectors for Calorimetry
- Developments for H1 at HERA -

G. Lindström, M. Eberle, I. Fedder, E. Fretwurst, U. Pein,
V. Riech, H. Schatz, M. Seidel, R. Wunstorf, C. Zeitnitz

I. Institut für Experimentalphysik, Universität Hamburg

N. Croitoru, R. Darvas, A. Seidman

Department for Electronic Engineering, Tel Aviv University

R. Böttger, H. Schölermann

Physikalisch Technische Bundesanstalt Braunschweig (PTB)

ISSN 0418-9833

NOTKESTRASSE 85 · 2 HAMBURG 52

To be sure that your preprints are promptly included in the
HIGH ENERGY PHYSICS INDEX ,
send them to the following address (if possible by air mail) :

DESY
Bibliothek
Notkestrasse 85
2 Hamburg 52
Germany

DESY 90-109 ISSN 0418-9833
September 1990

V INTERNATIONAL CONFERENCE ON INSTRUMENTATION FOR COLLIDING BEAM PHYSICS

Institute of Nuclear Physics, Novosibirsk, USSR, March 1990

SILICON DETECTORS FOR CALORIMETRY
— Developments for H1 at HERA —

G. Lindström, M. Eberle, I. Fedder, E. Fretwurst, U. Pein
V. Riech, H. Schatz, M. Seidel, R. Wunstorf, C. Zeitnitz
I. Institut für Experimentalphysik, Universität Hamburg, FRG *)

N. Croitoru, R. Darvas, A. Seidman
Department for Electronic Engineering, Tel Aviv University, Israel

R. Böttger, H. Schölermann
Physikalisch Technische Bundesanstalt Braunschweig (PTB), FRG

1. INTRODUCTION

The increasing interest in the application of silicon detectors for high energy physics experiments, especially for vertex reconstruction, has again been shown by a number of reports during this conference. Silicon detectors have also been successfully employed for particle identification [1,2]. On the other hand large area pad detectors may as well be used for calorimetry. For experiments at future colliders they would offer the most compact design and combine a direct charge readout with superior signal to noise ratio and fast response. The nice features of silicon instrumented calorimeters have been demonstrated by a number of test experiments. The SICAPO collaboration is presently undertaking detailed investigations with a large hadronic set up [3,4]. A survey on the feasibility of silicon calorimetry for the SSC was undertaken in the Tuscaloosa workshop [5]. Our group is responsible for the PLUG-calorimeter in the H1 experiment at HERA, which will fill the gap between the LAr forward calorimeter and the beam pipe. This angular range is extremely important since at HERA 800 GeV protons collide with 30 GeV electrons and thus an appreciable amount of transverse momentum and energy would otherwise be lost. Design criteria are outlined in [6,7,8]. Here we will concentrate on problems connected with detector technology and performance, radiation damage and MC-simulations.

2. DETECTOR TECHNOLOGY AND PERFORMANCE

In an extensive R & D program a new method for producing silicon detectors was developed, which combines the surface barrier technique with a planar process. This combination proved to be very suitable for the fabrication of large area detectors in a small scale laboratory. For calorimetric applications a very good thickness homogeneity, narrow insensitive edge zones and a long term operation stability at overbias voltage in laboratory ambients are essential. A detailed description of the design criteria and the fabrication process is given in [9]. As an example, fig. 1 shows the true mosaic structure obtainable with these

*) work supported in part by BMFT contract OS 5HH19 I

detectors. The homogeneity of the sensitive thickness and area is very important for the accuracy of the absolute energy calibration. For the H1 calorimeter it was e.g. decided to keep the needed precision within 1%. Fig. 2 shows that our detectors lie well within these limits. Dead areas are originating in the narrow SiO_2 rim needed for edge protection. It has to be assured that these partially insensitive zones constitute only a very small percentage of the overall detector area, as otherwise non affordable cracks would be the result. Therefore careful investigations have been performed with a proton micro beam, which was scanned across this edge zone (see [10]). For an operating voltage of 100 V the sensitive area extends laterally to a limit which is approximately 200 µm beyond the gold electrode (fig. 3). Including the corner space needed for the front contact the overall effective coverage of the mosaic structure is 96 %.

A typical diode characteristic of one of the detectors is displayed in fig. 4. As can be deduced from the voltage dependence of the capacitance, depletion is reached at 80 V. In the operating bias range beyond this value the detector current is quite low (appr. 200 nA) and the total noise stays practically constant at a value of 4500 e while the detector contribution is negligible (1600 e). Therefore the signal to noise ratio is governed only by the read out electronics. As a test one of our detectors was bombarded with minimum ionizing particles (fig. 5, [11]). Due to the larger capacitive noise of the preamplifier used in this case, a signal to noise ratio of 7 was reached. In the upper part of this figure it is also demonstrated that the detector response is practically independent of the bias beyond the depletion voltage. For complete charge collection this is of course to be expected but it should be emphasized that silicon detectors are in this respect far superior to liquid ionization chambers (TMP, LAr).

Two of the important features of any detector fabrication process are the success rate and long term stability, which are both responsible for the overall cost effectiveness. We accept all mounted detectors with a maximum reverse current of 1 µA at 100 V. Using this criterium the success rate of our process is about 60% so far. The average current value of all accepted detectors is 325 nA or 13 nA/cm^2 (fig. 6). This is regarded to be excellent. Also the long term stability does not establish any problem. The different contributions to the total current, resulting from the Shottky barrier, oxide silicon interface and bulk generation stay constant over a period of several months (fig.7).

The nice performance of our detectors has been proven in earlier test experiments with electromagnetic calorimeters [12,13,14] and recently in an application for a possible presampler [15]. Such a device, to be located directly in front of the main calorimeter, is especially useful if the dead material between the interaction point and the calorimeter leads already to an appreciable preshowering of incoming electrons. This causes a fluctuating energy loss and hence the electromagnetic energy resolution is worsened. However, the energy loss in the dead material is correlated with the number of secondaries crossing the presampler plane and thus the calorimeter response can be corrected. Such measurements were undertaken in connection with the H1 calorimeter tests at CERN. An appreciable improvement was obtained (table 1). If the thickness of the dead material is — as usual — much smaller than 1 λ,

hadrons do not produce any secondaries and are recorded in the presampler as mips only. The pronounced difference in the energy spectrum of the presampler response for electrons and hadrons can therefore be used for discriminating between these particles (fig. 8). Applying a reasonable energy cut one would e.g. obtain 90 % electron efficiency with only 4 % of all pions not being rejected (pion misidentification).

3. RADIATION HARDNESS

For all applications of silicon detectors at future colliders the severe radiation conditions impose a dominant problem on their survivability. In calorimeters the main source for radiation damage stems from neutrons with a spectrum centered around 1 MeV. Up to several 10^{13} n/cm^2 and year are e.g. to be expected at the SSC (see [5] and literature cited there). In addition in the forward region a strong charged particle component can result in a dose of up to 100 kGy. It is for these reasons that an appreciable amount of our R & D project was devoted to the investigation of such effects. Results have been published already in [7,9,10,16,17]. Here we report on some recent experiments.

3.1 Increase of Detector Current

Irradiations with monoenergetic neutrons, protons and electrons were performed in which a careful measurement of the particle fluence resp. dose was always ensured. The applied dosimetry is described elsewhere [9]. In fig. 9. we show the observed increase of the detector current as function of particle fluence, with respective dose scales in the case of protons and electrons. In previous experiments it was shown that the predominant part of the current increase is due to bulk generation only [9]. Also ΔI is strictly proportional to the fluence resp. dose Φ, if self annealing is applied properly. Therefore, with V being the detector volume we can define a current related damage rate α according to

$$\Delta I/V = \alpha \cdot \Phi \qquad (1)$$

From our measurements we obtain the values listed in table 2. A detailed comparison to results reported by other authors is contained in [9,16,17].

The large difference between the dose related damage rate for protons and electrons respectively is not surprising. The production of primary point defects is governed by the Coulomb interaction with the atomic nuclei and therefore depends on the particle type and energy in a much different way than the dose which is calculated from the energy deposition via ionization processes. As mentioned above the values plotted in fig. 9 and table 2 have been obtained after correcting for self annealing taking place during the irradiation and between irradiation and measurement. All values are also normalized to a temperature of 20° C. The importance of taking the self annealing effect into account is demonstrated in fig. 10. The different measurements were done with the same neutron flux and hence the irradiation time had to be increased to

obtain higher fluences. Only after correction of the original data for self annealing during irradiation a true proportionality between fluence and current increase is observed. A detailed investigation of the self annealing is reported in [9,16]. The measured dependence of α on the neutron energy coincides very well with the respective displacement damage cross section reported by the Sandia Corp. [18]. Assuming the neutron energy spectrum in the bulk of a hadronic calorimeter to be approximately equivalent to that of fission neutrons with an effective mean value of 1.2 MeV the effective damage rate is $8 \cdot 10^{-17}$ Acm^{-1}. Applying the same measures for annealing corrections and normalization to energy and temperature the values given by [19,20,21] are also lying in this range (between 6 and $10 \cdot 10^{-17}$ Acm^{-1}). On the basis of $\alpha = 8 \cdot 10^{-17}$ Acm^{-1} we would reach a current increase of 10 μA/cm^2 for a detector thickness of 400 μm at $3 \cdot 10^{12}$ n/cm^2. If self annealing is taken into account and the exposure extends over a period of a working year (100 days) the maximum tolerable fluence for such detector current would be $8 \cdot 10^{12}$ n/cm^2.

3.2 Donor Removal

Another important effect is the influence of radiation damage on the effective donor concentration N_{eff} respectively the material resistivity ρ. We observe a decrease of N_{eff} as function of the particle fluence Φ. For neutrons an example of our experimental results is shown in fig. 11. Again self annealing plays an important role, both during extended exposures as well as for the elapsed time durations between irradiation and measurement [22]. After correcting the data accordingly the decrease is however still not a linear function of the fluence. A possible explanation would be that most of the effect is due to the generation of vacancy phosphorus centers (V-P centers), as indicated by the work of Vismara [20]. The primary damage creates highly movable vacancies, which can then be trapped by the phosphorus donors. As the V-P centers are negatively charged we have a twofold influence on the effective space charge. The nonlinearity observed in fig. 11 would then be expected since the donor removal rate, defined as

$$\beta = dN_{eff}/d\Phi \qquad (2)$$

depends on the actual donor concentration [22]. The average value of β, extracted from fig. 11 (curve (b)), is about $5 \cdot 10^{-1}$ cm^{-1}. Therefore without any self annealing the donor removal leads to inversion of the conduction type at $1.5 \cdot 10^{12}$ n/cm^2 (see fig. 11). According to our preliminary results the maximum tolerable fluence for avoiding such inversion would be about $3 \cdot 10^{12}$ n/cm^2 reached in one working year of operation (100 days) if self annealing is taken into account. This result has however to be reconfirmed by further measurements.

3.3 Charge Collection Deficiency

Radiation damage not only influences the detector current and the effective

space charge but also leads to the generation of deep trapping centers. The consequence is an enhanced trapping of the charge carriers and hence a degradation of the energy calibration and resolution. We have studied this charge collection deficiency in detail by looking at the energy response to short ranged alpha particles incident on the front and rear side of the detector. Measuring the pulse height defect as function of the detector bias voltage, electron and hole trapping can be investigated separately [9]. An example is shown in fig. 12. The slope of these curves corresponds to the inverse of the trapping time constant. Here too we observe a self annealing effect, which is however pronounced only in the case of electrons. Using the extracted trapping time constants the charge collection deficiency $\Delta Q/Q_0$ for minimum ionizing particles was calculated as function of the neutron fluence Φ. We get:

$$\Delta Q/Q_o = \gamma \cdot \Phi \qquad (3)$$

with a value of $\gamma = 2.8 \cdot 10^{-15}$ cm^2. Therefore a charge collection deficiency of 1% is reached at $3.6 \cdot 10^{12}$ n/cm^2. As the hole trapping is mostly responsible for the observed overall degradation this maximum tolerable fluence is not changed appreciably if self annealing is taken into account.

3.4 Temperature Enhanced Annealing

In the preceding paragraphs we have seen that the maximum neutron fluence which may be tolerated without reaching an excessive current, charge collection deficiency or inversion of the conduction type is in the order of $5 \cdot 10^{12}$ n/cm^2 and working year (100 days). This is an order of magnitude less than to be expected in the very forward regions of future collider experiments. In order to ensure the survivability of the detectors one therefore has to rely on special annealing methods. So far we have applied certain heat cycles, which are partly described in [9,16]. In table 3 we summarize some of the more recent investigations, which we have started in order to optimize the temperature dependence of the annealing. The results are somewhat preliminary, since due to experimental difficulties the heat treatment was done after an appreciable self annealing had taken place already. Also the measurements for ΔI, ΔN and ΔQ before heat treatment belong in general to different detectors with different individual times elapsed for self annealing. But apart from these unsystematics the overall behaviour may be described as follows. After a one hour heating at 200° C we get a very nice further decrease of the current by a factor of 3.5. Hence the initially damage induced current is reduced to 10%. Such a heat treatment helps therefore very much to recover the operability of a detector as far as the current is concerned. However we get a reverse effect for the change in the effective donor concentration. While self annealing has helped to regain some of the donor concentration lost due to radiation damage (see fig. 11) the heat treatment leads to an increase of ΔN again. As far as the charge collection deficiency is concerned we get an improvement in case of the electrons while the observed degradation for the hole contribution stays small only at 140°C. However even at 200°C the overall effect on mips is still below 1% and may therefore be tolerable. From table 3 it is clear that a further optimization of the

heat treatment has to be done. A temperature of 200°C would be highly desirable as far as the improvement of the current is concerend but seems to be prohibitive as to the involved donor removal. Further studies are under way.

Enhanced annealing by heat treatment or any other method is only meaningful, if the detectors are afterwards to be used again. We may then ask the question how many damage annealing cycles they can survive extending their operability over much longer times than otherwise possible. A preliminary answer is given in fig. 13. We used two irradiations with 1 and $3 \cdot 10^{12}$ n/cm^2 respectively followed by heat treatments at 200°C for one hour each. As to be expected from fig. 11 and table 3 we get inversion after an integral fluence of $4 \cdot 10^{12}$ n/cm^2 during the second annealing. As to the detector current the annealing in the first step and the increase again during the second irradiation is also as to be expected. The increase during the second annealing can certainly be attributed to the material inversion and may be avoidable if a different process for the rear contact is used. Finally, the charge collection deficiency shows the expected trend too, i.e. an increase not only due to radiation damage but an additional worsening during annealing. Though the second annealing hints a small improvement this is not regarded to be real. The material inversion affects the evaluation from the alpha particle measurements. An improved analysis taking the actual electric field distribution into account will probably result in seeing a further degradation.

3.5 Defect Characterization

For the actual application of silicon detectors under the severe conditions of intense radiation fields the influence of radiation damage on the detector properties as surveyed above is most important. If one wants however to improve their radiation hardness by optimizing the material selection, process technology or annealing method a better understanding of the defects responsible for the observed degradation is essential. It has been shown that the DLTS method (deep level transient spectroscopy, introduced by Lang [23]) is a very powerful tool for such investigations [20,24,25,26,27]. Presently we have started own measurements with a DLTS apparatus available at the University of Tel Aviv. Some first results are shown in fig. 14. Fig. 14a shows an example of the observable capacitive transient as function of temperature. The observed peaks in such a spectrum belong to different defect sites respectively their individual energy levels in the forbidden gap. If measured for various time windows t_1, t_2 one can extract an emission rate e as function of the absolute temperature T. A suitable plot of e versus T (Arrhenius plot) leads finally to the activation energy. An example of such a plot is shown in fig. 14b. The activation energies are given in comparison to results of other authors in table 4. It should be pointed out that our analysis gives a clear identification of the involved defect sites. In addition to the well known vacancy-oxygen center (V-O) and the double charge state of the divacancy ($V\text{-}V^{=}$) we have been able to resolve the single charge state divacancy ($V\text{-}V^{-}$) from the vacancy phosphorus (V-P) complex. This will be very helpfull in understanding the different reported degradation and annealing effects. Further work is in progress.

4. MONTE CARLO STUDIES FOR SILICON INSTRUMENTED CALORIMETERS

In a previous paper we have emphasized that realistic simulations for the electromagnetic response of silicon instrumented calorimeters can only be obtained if special attention is paid to the very small detector thickness [14,28]. EGS4 leads to an excellent agreement with experimental results, provided the relevant parameters are optimized. Very low values (e.g. ESTEPE = 1%, ECUT = 10 keV) were necessary since low energetic electrons play a very important role for the energy response of a silicon calorimeter. While 20% of all particles crossing a silicon plane in an electromagnetic shower have an energy of less than 1 MeV, they produce 40% of the total visible energy. The importance of soft electrons for the response of a silicon instrumented hadron calorimeter was emphasized by various reports of the SICAPO collaboration [3,4,5,29]. Here we will concentrate on some recent results obtained with GEANT 3.13. In a first step we tried to varify the EGS4 results for the spectral response of a silicon detector if bombarded by monoenergetic electrons. The choice of parameters was taken from our EGS4 experience but in addition it proved necessary to choose the LOSS3 version as only here the explicit generation of delta rays allows a realistic calculation of the restricted energy loss. The program had also to be modified slightly such that multiple scattering (Moliere algorithm was chosen) is calculated for each step. The original GEANT version applies the multiple scattering correction only every half radiation length or at a boundary between two different media. This leads to large errors in case of electrons. After these modifications had been introduced, GEANT gives a similarly nice reproduction of the experimental energy loss spectrum as could be achieved with EGS (see fig. 15). Table 5 summarizes some experimental results obtained with a Cu/Si-calorimeter (1 X_0 sampling, 400 µm Si) in comparison to relevant MC calculations. Though the agreement in the case of the modified GEANT version (internal name: GEANT 3.13S) is not quite as good as was obtained with EGS4 it is much better than achievable with the original version (GEANT 3.13).

With respect to hadronic showers we concentrated so far on the neutron spectrum and flux distribution. A better understanding is here regarded to be essential for a possible geometry optimization and a realistic estimate of detector degradation effects induced by neutron damage. In additon to the above mentioned GEANT modifications we found it necessary to use double precision variables in some subroutines (meanwhile implemented in the official GEANT code source) in order to avoid rounding errors. Also the calculation of neutron nucleus scattering was improved [31]. Fig. 16 shows the GEANT results in comparison with CALOR for a special Fe/Si-calorimeter [32]. The MORSE neutron transport code contained in CALOR is expected to follow the neutron propagation down to low energies quite well. This comparison may therefore be taken as a reliability check for GEANT. As can be seen the neutron spectra (at shower maximum) coincide pretty well at energies above 1 MeV. For lower values GEANT simulates less intensity than CALOR. Apart from an overall scaling factor originating probably from this discrepancy the longitudinal distribution of the neutron flux is identical for both simulations (fig.17). Further work including calculations of the visible energy, e/h-ratio and energy resolution as well as a comparison with the HERMES code is in progress.

5. REFERENCES

[1] M. Turala, Proc. XXIV Int. Conf. on High En. Phys., Munich 1988, 1240
[2] C. Gößling, Proc. XXIV Int. Conf. on High En. Phys., Munich 1988, 1208
[3] E. Borchi et al., Nucl. Instr. and Meth. A 279 (1988) 57
[4] F. Lemeilleur et al. IEEE Trans. Nucl. Sci. Vol. 36,1 (1989) 331
[5] J. E. Brau ed., Summary Report, Silicon Calorimetry Working Group, Workshop on Calorimetry for the Superconducting Super Collider, Tuscaloosa/Alabama March 1989; OREXP-89-0902 and to be published
[6] H1 collaboration, Technical Proposal for the H1 Detector (1986) 117
[7] G. Lindström et al., in Proc. Conf. on High Energy Exp. and Methods HEXAM 89, Bechyne CSSR 1989, p. 76
[8] E. Fretwurst et al., Proc. ECFA Study Week on Instrum. Techn. for High Luminosity Hadron Colliders, Barcelona 1989; ECFA 89-124, 1 (1989) 319
[9] E. Fretwurst et al., Nucl. Instr. and Meth. A 288 (1990) 1
[10] E. Fretwurst et a., Nucl. Instr. and Meth. A 253 (1987) 467
[11] Y. Kamishkov, ITEP; private communication
[12] M. Bormann et al., Nucl. Instr. and Meth. A 240 (1985) 63
[13] M. Bormann et al., Nucl. Instr. and Meth. A 257 (1987) 479
[14] G. Lindström et al., MC-Simulations with EGS4 for Calorimeters with Thin Silicon Detectors; Workshop on Calorimetry for the Superconducting Super Collider, Tuscaloosa/Alabama, March 1989
[15] C. Zeitnitz et al., Verhandl. DPG (VI) 25,1 (1990) 20; Ann. Report 1988/89, Ist Inst. f. Exp. Phys. Univ. of Hamburg, FRG (1990)
[16] G.Lindström et al., Radiation Damage Effects in Silicon Detectors; Workshop on Calorimetry for the Superconducting Super Collider, 1989
[17] R. Wunstorf et al., Proc. ECFA Study Week on Instrum. Techn. for High Luminosity Hadron Colliders, Barcelona 1989; ECFA 89-124, 1 (1989) 321
[18] Techn. Report SAND87-0098 Vol.1, Sandia Natl. Lab. 1987
[19] T. Ohsugi et al., Contr. to the Workshop on Calorimetry for the Superconducting Super Collider, Tuscaloosa 1989; HUPD-8903 (1989)
[20] L. Vismara et al., Contribution to the Workshop on Calorimetry for the Superconducting Super Collider, Tuscaloosa/Alabama 1989, reported in [5]
[21] H.W. Kraner et al., Nucl. Instr. and Meth. A 279 (1989) 266
[22] M. Benkert, Diploma Thesis Univ. of Hamburg 1990 and to be published
[23] D.V. Lang, J. Appl. Phys. 45 (1974) 3023
[24] G.L. Miller et al., Ann. Rev. Mat. Sci. 30 (1977) 377
[25] E. Borchi et al., Nucl. Instr. and Meth. A279 (1989) 277
[26] Y. Tokuda et al., IEEE Trans. Nucl. Sci. NS-28 (1981) 3564
[27] L. Tulach et al., Phys. Status Solidi (a) 100 (1987) K13
[28] M. Eberle et al., Internal Report H1-05/89-113 (1989)
[29] F. Lemeilleur et al., Phys. Lett. B222 (1989) 518
[30] M.J. Berger et al., Nucl. Instr. and Meth. 69 (1969) 181
[31] I. Fedder et al., Verhandl. DPG (VI) 25, 1 (1990) 59 and Ann. Report 1988/89, Ist Inst. f. Exp. Phys., Univ. of Hamburg, FRG (1990)
[32] K. Furuno et al., OREXP-89-0901, University of Oregon, USA (1989)

Table 1 Influence of the presampler correction on the energy response of the LAr calorimeter for electrons.

E [GeV]	Q [pC]	σ [pC]	σ/√E	comment
10	2.14 (-12%)	0.209	30.9%	1.5 Xo in front no correction
10	2.40 (-1%)	0.159	20.9%	1.5 Xo in front corrected with Si-plane
10	2.42	0.120	15.7%	no material in front
30	6.91 (-8%)	0.314	24.9%	1.5 Xo in front no correction
30	7.32 (-3%)	0.238	17.8%	1.5 Xo in front corrected with Si-plane
30	7.54	0.188	13.7%	no material in front
50	11.90 (-5%)	0.434	25.8%	1.5 Xo in front no correction
50	12.44 (-1%)	0.287	16.3%	1.5 Xo in front corrected with Si-plane
50	12.56	0.241	13.6%	no material in front

Table 2 Current related damage rate α for neutrons, protons and electrons.

particle type	energy [MeV]	damage rate α(T=20 °C) $[10^{-16}A/cm]$	$[10^{-9}Acm^{-3}Gy^{-1}]$
neutron	14.1	1.47 ± 0.09	——
neutron	5.0	1.36 ± 0.04	——
neutron	1.2	0.79 ± 0.03	——
proton	21.1	2.09 ± 0.10	65.7 ± 3.1
electron	1.8	$4 \cdot 10^{-4}$	0.15

Table 3 Annealing influence on the detector current, effective donor concentration and charge collection deficiency.

heat treatment (1 hour)		$\Delta I / \Delta I_0$ [%]	$\Delta N / \Delta N_0$ [%]	$\Delta Q / Q_0$ for mip's [%] electrons	holes	total
140 °C	before	31	48	0.17	0.50	0.67
	after	14	68	0.08	0.53	0.61
180 °C	before	31	48	0.13	0.38	0.52
	after	8	92	0.04	0.62	0.66
200 °C	before	32	50	0.07	0.30	0.37
	after	9	119	0.03	0.81	0.84

Table 4 Results of DLTS measurements for activation energy of different defect sites.

	ENERGY LEVEL [eV] V-O	V-V⁼	V-V⁻	V-P
Miller [23]	0.18	0.23	0.39	0.44
Borchi [24]	0.16	0.25	0.40	
Tokuda [25]	0.15	0.21	0.39	
Tulach [26]	0.18	0.25	0.46	
this work	0.18	0.24	0.39	0.45

Table 5. Visible energy and energy resolution obtained with a Cu/Si-calorimeter for 4 GeV electrons. Comparison of experimental data and GEANT simulation.

GEOMETRY	E_{vis} [MeV]	(σ/E)√E [%√GeV]	REDUCTION
EXPERIMENT			
without G10	27.43 ± 0.32	25.9 ± 0.6	—
1.5 mm G10 front	26.12 ± 0.36	24.8 ± 0.6	4.7%
1.5 mm G10 rear	25.32 ± 0.32	25.1 ± 0.6	7.6%
1.5 mm front and rear	24.48 ± 0.28	24.5 ± 0.6	10.7%
EGS4			
without G10	26.80 ± 0.04	23.9 ± 0.3	—
1.5 mm G10 front	25.64 ± 0.08	22.7 ± 0.3	4.3%
1.5 mm G10 rear	24.84 ± 0.08	23.3 ± 0.4	7.3%
1.5 mm front and rear	23.60 ± 0.08	22.7 ± 0.5	11.9%
GEANT 3.13			
without G10	29.53 ± 0.18	23.6 ± 1.0	—
1.5 mm G10 front	25.72 ± 0.15	23.0 ± 1.0	12.9 ± 0.7%
1.5 mm G10 rear	27.89 ± 0.17	25.0 ± 1.1	5.6 ± 0.8%
1.5 mm front and rear	24.88 ± 0.16	23.5 ± 1.1	15.7 ± 0.7%
GEANT 3.13 S			
without G10	26.14 ± 0.18	22.8 ± 1.1	—
1.5 mm G10 front	25.01 ± 0.22	22.6 ± 1.5	4.3 ± 1.7%
1.5 mm G10 rear	24.03 ± 0.20	24.8 ± 1.5	8.1 ± 1.0%
1.5 mm front and rear	23.86 ± 0.37	29.7 ± 2.9	8.7 ± 1.5%

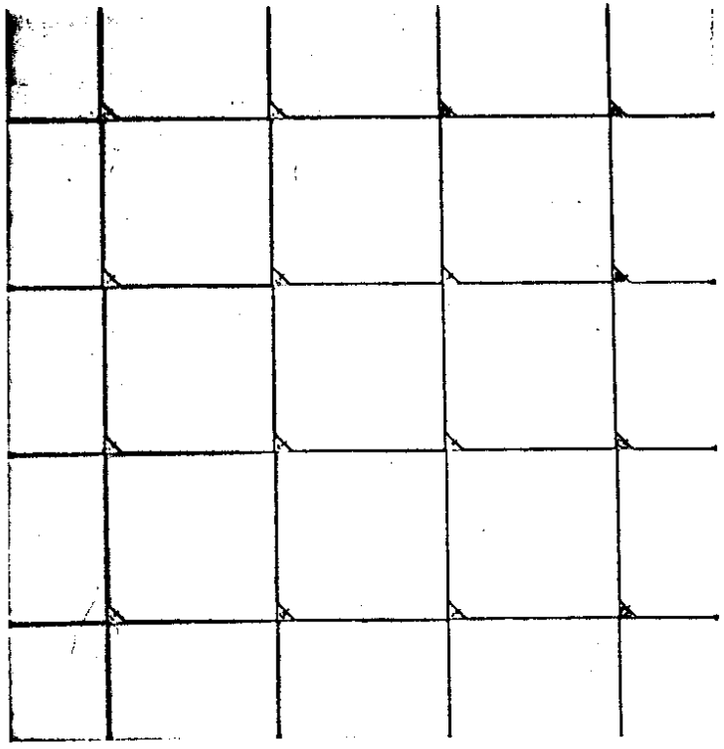

Fig. 1 Detail of a true mosaic plane with 5×5 cm^2 silicon detectors.

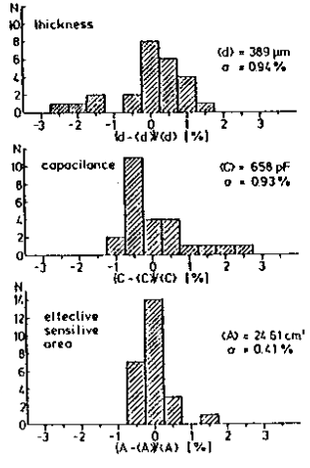

Fig. 2 Homogeneity of detector thickness, capacitance at 100 V. and effective sensitive area.

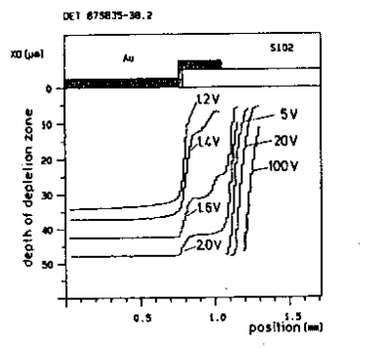

Fig. 3 Extension of the depletion zone near the electrode edge.

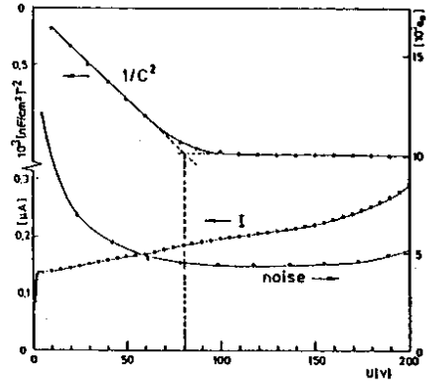

Fig. 4 Typical I, C and noise characteristics of an HI - Si - detector.

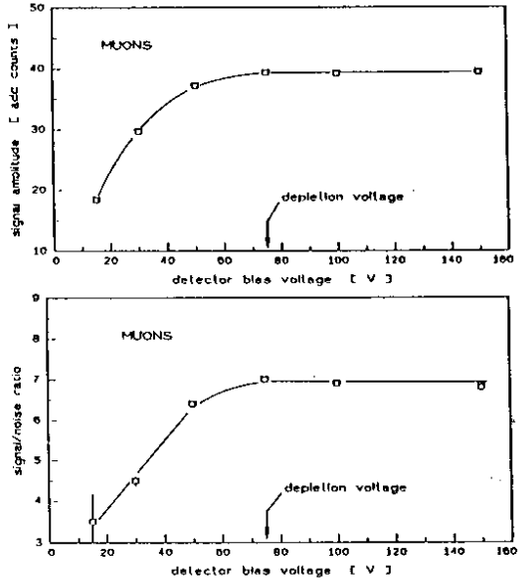

Fig. 5 Plateau curves of the signal amplitude and signal to noise ratio for muons in 400 µm silicon.

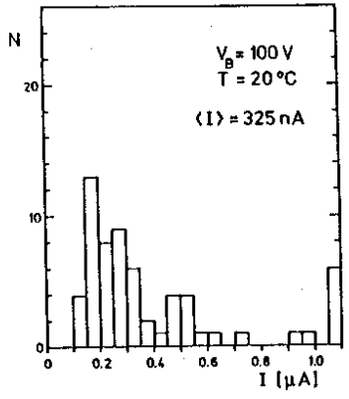

Fig. 6 Current distribution of fully depleted detectors.

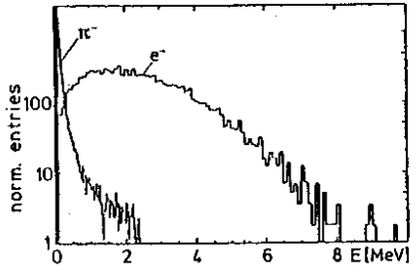

Fig. 8 Spectrum of deposited energy for 30 GeV electrons and pions in 400 μm silicon behind 1.5 X_0 absorber material.

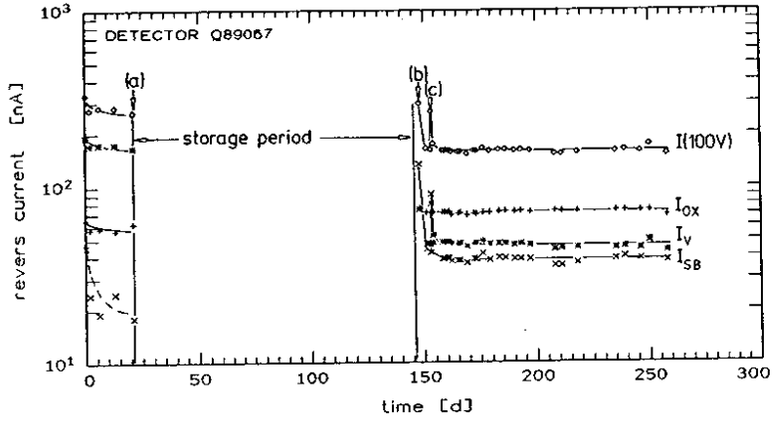

Fig. 7 Time dependence of different contributions to the detector current.
(a) protection varnich applied for cutting
(b) cutting and mounting
(c) surface protection

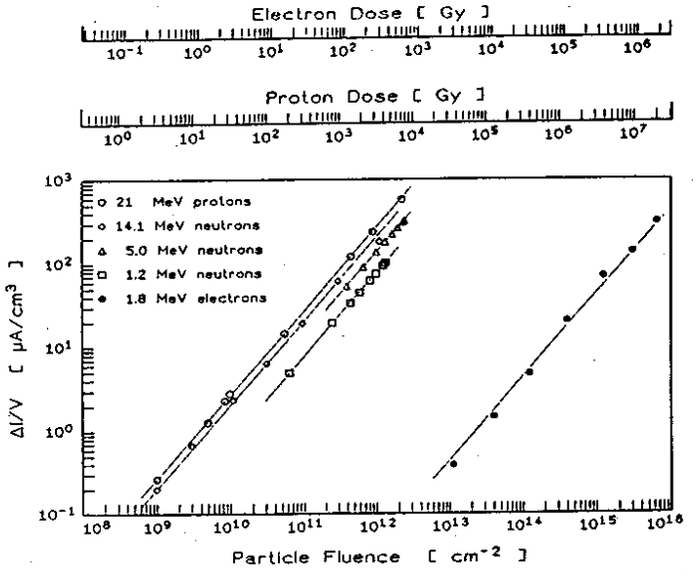

Fig. 9 Increase of measured bulk generation current as function of particle fluence.

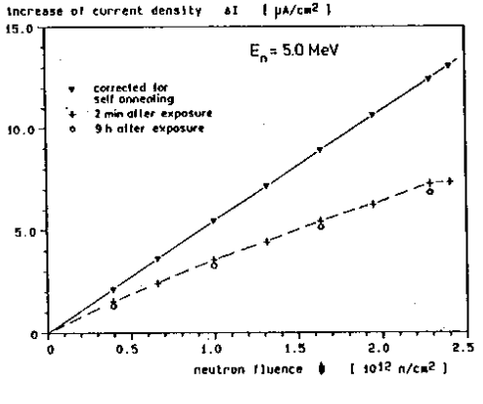

Fig. 10 Current increase versus neutron fluence, measured values and corrected for self annealing.

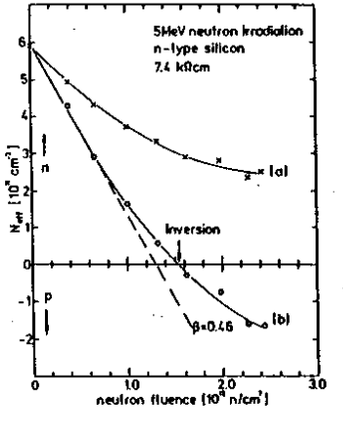

Fig. 11 Reduction of effective donor concentration as function of neutron fluence, measured values and corrected for self annealing.

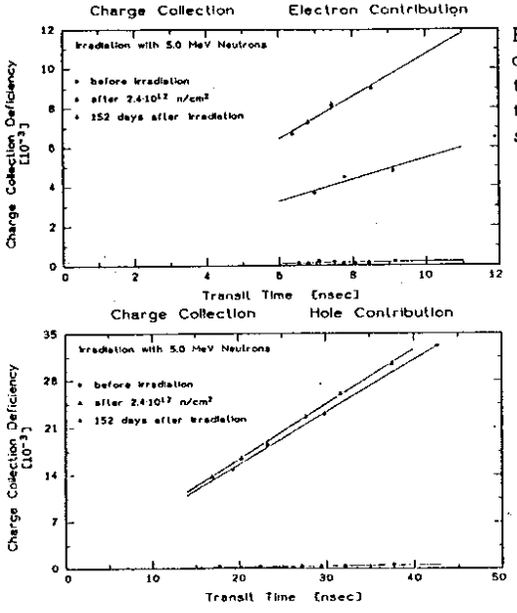

Fig. 12 Charge collection deficiency versus transit time before and after neutron irradiation and after self annealing.

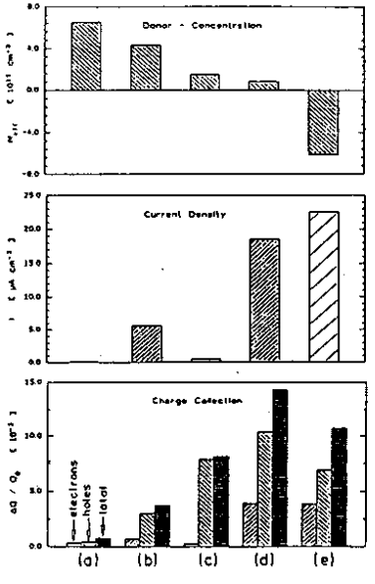

Fig. 13 Effect of successive damage and thermal annealing (a) before irradiation, (b) after first irradiation ($1 \cdot 10^{12}$ n/cm^2), (c) after first heat treatment (200°C, 1 h), (d) after second irrad. ($3 \cdot 10^{12}$ n/cm^2), (e) after second treatment (200°C, 1 h).

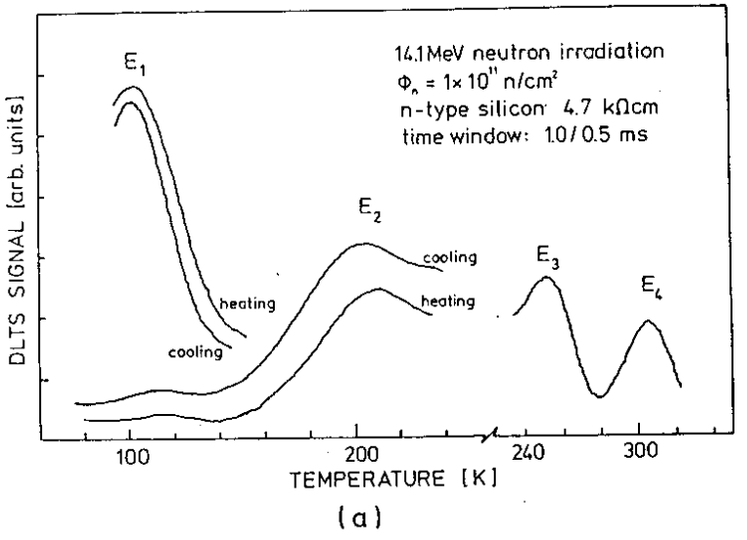

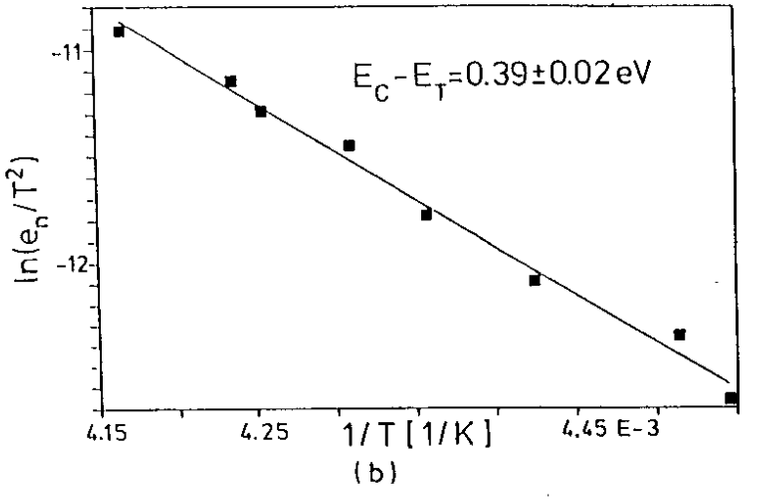

Fig. 14 DLTS results for a neutron irradiated silicon detector
(a) DLTS-spectrum;
(b) Arrhenius plot for the single charged divacancy.

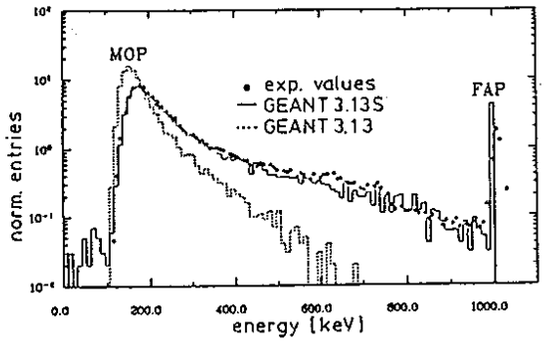

Fig. 15 Comparison of measured and simulated energy deposition in 530 µm silicon for 1 MeV electrons (experimental points see [30]).

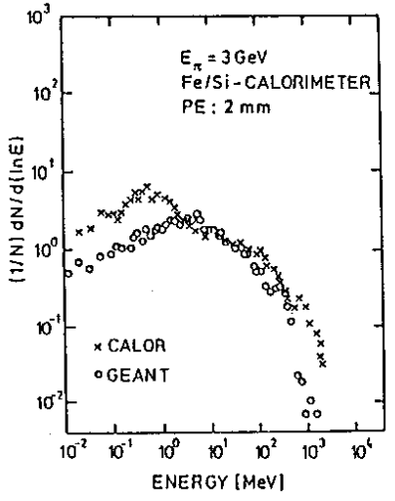

Fig. 16 Comparison of neutron energy spectrum at shower maximum simulted with CALOR and GEANT.

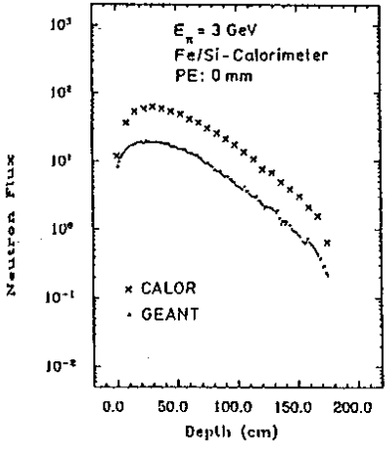

Fig. 17 Comparison of longitudinal neutron flux development simulated with CALOR and GEANT.